ACS OMEGA

http://pubs.acs.org/journal/acsodf

Article

Theoretical Study on the Swelling Mechanism and Structural Stability of Ni_3Al-LDH Based on Molecular Dynamics

Xiaoliang Wang,* Leiming Chang, Haonan Zhao, Zhenqiu Yu, Yingkai Xia, Chuanhui Huang, Shaobin Yang,* Guoxiang Pan, Shengjie Xia, Yi Liu, and Jingxin Fan

Cite This: *ACS Omega* 2023, 8, 3286−3297

Read Online

ACCESS | Metrics & More | Article Recommendations | Supporting Information

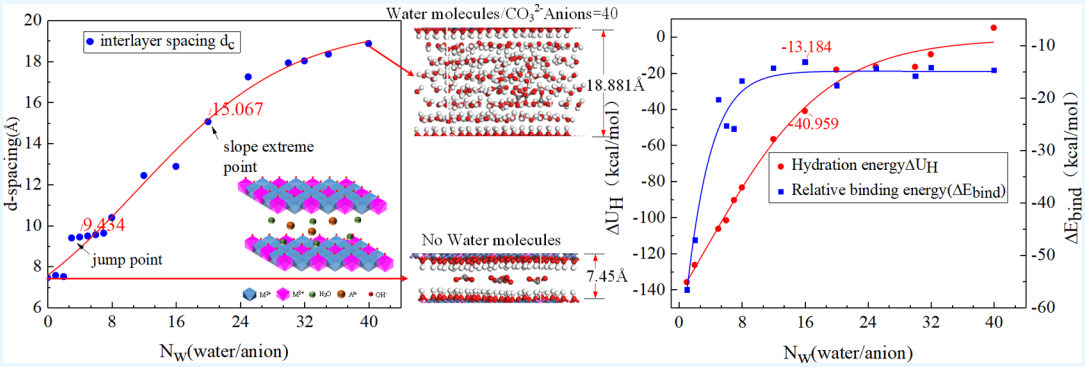

ABSTRACT: layered double hydroxide (LDH) as a kind of 2D layer material has a swelling phenomenon. Because swelling significantly affects the adsorption, catalysis, energy storage, and other application properties of LDHs, it is essential to study the interlayer spacing, structural stability, and ion diffusion after swelling. In this paper, a periodic computational model of Ni_3Al-LDH is constructed, and the supramolecular structure, swelling law, stability, and anion diffusion properties of Ni_3Al-LDH are investigated by molecular dynamics theory calculations. The results show that the interlayer water molecules of Ni_3Al-LDH present a regular layered arrangement, combining with the interlayer anions by hydrogen bonds. As the number of water molecules increases, the hydrogen bond between the anion and the basal layer gradually weakens and disappears when the number of water molecules exceeds 32. The hydrogen bond between the anion and the water molecule gradually increases, reaching an extreme value when the number of water molecules is 16. The interlayer spacing of Ni_3Al-LDH is not linear with the number of water molecules. The interlayer spacing increases slowly when the number of water molecules is more than 24. The maximum layer spacing is stable at around 19 Å. The interlayer spacing, binding energy, and hydration energy show an upper limit for swelling: the number of water molecules is 32. When the number of interlayer water molecules is 16, the water molecules' layer structure and LDH interlayer spacing are suitable for anions to obtain the maximum diffusion rate, 10.97×10^{-8} $cm^2 \cdot s^{-1}$.

1. INTRODUCTION

Layered double hydroxide (LDH), also known as anionic clays or hydrotalcite,[1] is a class of inorganic functional materials with a layered structure, which can form a large type of structurally similar anionic layered materials by modulating the composition of the basal layers and the interlayer ions and molecules (Figure 1 for the structure). It has been widely studied in energy storage and conversion,[2] controlled-release drugs,[3] catalysis,[4] sensors,[5] and environmental protection.[6] With the progress of modern testing methods and the expansion of cross-disciplinary research, LDHs have found new applications in functional polymer materials, cosmetics, and other fine chemicals,[7,8] demonstrating a broader application prospect.

The physical or chemical role of LDH interlayer active sites is required for energy storage and conversion, controlled drug release, catalysis, magnetic energy, ion adsorption, and other fields.[9−14] The large interlayer spacing is necessary to accelerate the molecular and ionic guests into the interlayer for ion exchange or chemical reaction and improve the performance of LDHs. Usually, inorganic anions intercalate LDH with small interlayer spacing, slow ion transport rates between layers, and underutilization of interlayer active sites. Therefore, improving the electrochemical performance by expanding the interlayer spacing of LDHs, improving the ion transport kinetics, enhancing the multiplicative capacity,[15] and activating more electrochemically active sites in the inter-

Received: October 25, 2022
Accepted: December 23, 2022
Published: January 10, 2023

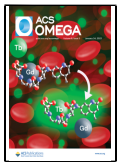

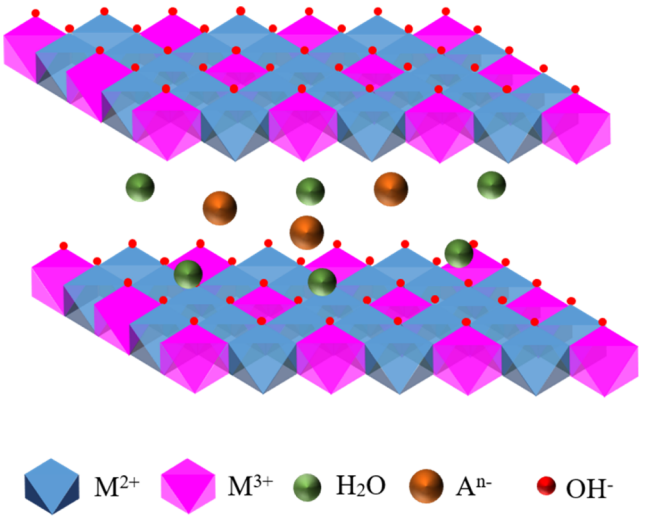

Figure 1. Schematic diagram of the layered structure of LDHs.

layer[16−19] have become an important research topic. Large-size anion intercalation is usually used to expand the interlayer spacing of LDHs. Xiao et al.[20] prepared CoAl-A-LDH with interlayer spacings of 0.76, 0.87, and 2.58 nm in order by the hydrothermal method using CO_3^{2-}, SO_4^{2-}, and dodecyl sulfate as intercalation anions. The CoAl(DS^-)-LDH sample with the largest interlayer spacing (2.58 nm) has the smallest charge transfer and diffusion resistance, which is better than the samples with interlayer spacings of 0.76 and 0.87 nm. Lin et al.[21] produced NiCo-LDH with an interlayer spacing of 1.53 nm by the hydrothermal method using dodecylbenzene sulfonate as an intercalation anion. The specific capacities at current densities of 3 and 10 $A{\cdot}g^{-1}$ were 1646 and 680 $F{\cdot}g^{-1}$, which is much better than the control sample with an interlayer spacing of 0.72 nm. It is shown that the expanded interlayer spacing could effectively improve the electrochemical properties of LDH. Ding et al.[22] investigated the effective adsorption of two anionic intercalated LDH from water to remove F-53B harmful substances. The results showed that SDS-LDH exhibits higher adsorption performance than NO_3^--LDH. This is mainly due to the presence of SDS in the interlayer, which leads to a larger interlayer spacing and increased surface area of SDS-LDH. Zhang et al.[23] systematically controlled the interlayer spacing by inserting n-alkyl sulfonates of different carbon numbers. They investigated the magnetic properties using temperature- and field-dependent magnetization measurements, showing that increasing the interlayer spacing changes the competition between in-plane superexchange and remote out-of-plane dipole interactions.

In a previous study, our group inserted large-sized anions into the interlayer to increase the interlayer spacing effectively. It explored the effect of the average interlayer spacing on the electrical performance of NiMn-LDH.[24] It was also found that the aqueous environment in which LDHs are located will cause swelling of LDHs and increase interlayer spacing, a common phenomenon for LDHs. However, swelling occurs in a solution environment, and the relevant information cannot be obtained experimentally. At the same time, the simulation is easier to get the local interlayer spatial microscopic information when swelling occurs.[25] Related studies have seen some reports. For example, Murthy et al.[26] used molecular dynamics and density functional theory simulations to construct a computational model of CrO_4^{2-} and VO_4^{3-} insertion MgAl-LDH interlayer after inserting different numbers of water molecules to study the structural parameters, hydrogen bonding, hydration energy, self-diffusion coefficients, and so forth. Costa et al.[27−29] found that the intercalating anions slightly distort the hydroxyl groups in LDH basal layers relative to the hydro-magnesite structure and that the anions and water molecules are arranged in a monolayer film shape among the layers, which has a significant effect on the interlayer spacing; the more strongly bound anions are those with smaller ionic radii, causing a decrease in the interlayer spacing; the electron density in the interlayer region decreases during dehydration, inducing the migration of Cl^- anions and the displacement of hydroxyl layers from adjacent layers, and that these structural changes are designed to restore some of the hydrogen bonds broken due to the removal of water molecules. Molecular dynamics simulation by Chen et al.[30] showed that in LDH ($Mg_2Al(OH)_6Cl^-{\cdot}mH_2O$), water molecules are mostly fixed at hydroxyl positions and enclosed monolayers, acting as acceptors for hydrogen bonds provided by both upper and lower hydroxyl groups, and diffuse in a similar way to atoms in a solid lattice.

Although the relationship between layer, interlayer water, and interlayer anion of LDHs has been investigated in previous simulation studies, for example, Marappa and Vishnu Kamath[31] experimentally considered the interaction between anion hydration in layered bimetallic hydroxides and water in the interlayer. The water content related to the hydration of the anion was finally determined through a series of thermogravimetric analyses. It was found that the water molecules between the layered double hydroxide layers were distributed between the hydrocarbon group on the metal hydroxide layer and the inserted anion. When the anion was CO_3^{2-}, the required water molecule content was highest. However, what is the generation law of interlayer swelling, and how are the intercalation anions and water molecules lined up with LDHs? What are the effects of swelling behavior on interlayer spacing, structural stability, and ion diffusion? The effect of interlayer water molecular weight N_w (the ratio of the number of interlayer water molecules to the number of anions) on swelling behavior, stability, and ion diffusion has not been disclosed. Moreover, Ni_3Al-LDH, with excellent performance in energy storage, conversion, and catalysis, has not been reported in studies on swelling. Therefore, this paper developed the molecular dynamics[32] (MD) model of the Ni_3Al-LDH structure containing interlayer water molecules and ionic column support structure. In this paper, the role of water molecules inserted into the layers is further studied, and the specific distribution state of water molecules between layers and the interaction between water molecules and anions and layers can be more intuitively displayed according to the calculation results of molecular dynamics. The XRD spectrum was simulated to compare with the experimental characterization results and continuously optimize the model. The influence of interlayer guest size, the guest arrangement, and interlayer water molecular weight on interlayer spacing, system formation energy, and spatial structure was studied. Combined with the experimental data, the swelling and structural stability law of LDHs is analyzed to provide a theoretical basis for synthesizing LDHs with an optimized interlayer complex structure.

https://doi.org/10.1021/acsomega.2c06872
ACS Omega 2023, 8, 3286−3297

2. CALCULATION MODEL AND METHOD

2.1. Calculation Model. All simulations were performed using the Forcite module of the Material Studio 2019 package. The space group of Ni_3Al-A-LDH was performed with $P6_3/mmc$ (no. 194), and stacking was performed in 2H with Ni/Al of 3:1. The calculations have shown that the three oxygen atoms of the CO_3^{2-} anion are H-bonded with hydroxyl groups of the hydroxide layer that results in the lowest energy (highest stability) of the horizontal orientation of CO_3^{2-} to the basal layer and hampers the ion exchange.[33] In this way, the LDH stability depends on the binding mode and mobility of CO_3^{2-}. Therefore, it is useful to find conditions for the diffusion of CO_3^{2-} and we choose it as the interlayer anion. The initial state takes water molecules randomly distributed in the interlayer space. The lattice parameters a, b, and c were measured concerning powder X-ray diffraction of LDHs. In this paper, $a = b = 3.055$ Å, $c = 7.86$ Å; $\alpha = \beta = 90.0°$, $\gamma = 120.0°$.[33] Super units of each Ni_3Al-A-LDH are $8 \times 4 \times 1$ in the a, b, and c directions. Based on the abovementioned parameters, a model with only CO_3^{2-} intercalation between layers and Ni_3Al-CO_3^{2-}-LDH with different numbers of randomly distributed water molecules between several layers is established.

2.2. Calculation Method. Simulations of several force fields were performed according to the force field conditions selected by Pan et al.[34] The calculation results show that the optimization of DREIDING force field fails (force field parameters excluding Ni); the optimized structures obtained with COMPASS, CVFF, and PCFF force fields have poor symmetry and large deformation in the layer structure, and there is a staggered position between the upper and lower layer. While the optimized structure obtained using the UFF[35] has a regular and orderly arrangement of atoms (as showed in Figure S1). The layer spacing of 0.75 nm obtained by UFF is close to the experimental value of 0.786 nm, and so, UFF is suitable for the structural simulation of the hydrotalcite system. Therefore, the universal force field was used for all MD simulations.[36] The established model is first structurally optimized for energy minimization. Then, using the twofold structure optimization algorithm, the steepest descent is used for the first time, and the conjugate gradient is used for the energy minimization calculation for the second time, which contributes to the accuracy of the optimization. An annealing treatment follows this to allow the system to reach a steady state more quickly and facilitate the following kinetic calculations. The charge calculation was performed using the charge balance method (Q_{eq}),[37] and the temperature and pressure control was achieved using the Andersen heat bath and Berendsen heat bath[38] methods, respectively. The long-range electrostatic interaction was calculated using the Ewald summation method, and the Van Der Waals force was chosen from the atom-based method.[39] The cut-off distance is determined to be 8 Å, and the time step is 1 fs.[40] The accuracy of this calculation is chosen to consider the need for accuracy on the one hand and the optimization of calculation cost and time on the other hand. Since this experiment is to study the effect of hydrotalcite insertion into water molecules, a relatively suitable cut-off distance parameter was determined by the error analysis of hydrotalcite layer spacing and hydration energy. From Tables S1 and S2, we can see that both errors are about 0.5% as the cut-off distance increases, and so, the result of choosing 8 Å as the cut-off radius for this calculation has shown customer reliability. The calculations are based on a relaxation simulation of the isothermal-isobaric (NPT) ensemble at 50 ps (equivalent to 50,000-time steps) and a structural simulation of the NVT ensemble at 200 ps, with a temperature set to 300 k. The first part is an equilibrium simulation under the NPT ensemble with a total equilibrium time of 50 ps, which is used to calculate cell parameters, hydration energy, and binding energy. The hydration and binding energies are calculated as the result of equilibrium after 50 ps. To improve the accuracy of the cell parameter calculation, this paper is calculated by averaging the cell parameters, that is, taking the average of the sum of the cell parameters for each step number in the next 20 ps.[41] According to Zhao et al.,[42] it was found that the energy and lattice parameters of the system remained almost constant after the 200 ps simulation, indicating that the equilibrium state could be reached within 200 ps. We conducted similar simulations at 200, 250, 500, and 1000 ps and again found that the balance could be achieved within 200 ps (as shown in Table S3 and Figure S2). Our paper uses the first 50 ps as the equilibrium time based on the application in literature and only calculates the mean squared displacement for the last 150 ps. The 200 ps molecular dynamics simulation is based on the structural model calculated for the 50 ps NPT simulation. A detailed structural analysis of selected hydration levels at 300 K is presented in this paper.

3. RESULTS AND DISCUSSION

Several established models were selected for XRD simulation for comparison with literature.[43] The Ni_3Al-CO_3^{2-}-LDH (003) peak at 11.85° and (006) peak at 23.85° correspond well with the experimental data[44,45] (as showed in Figure 2). In Figure 2,

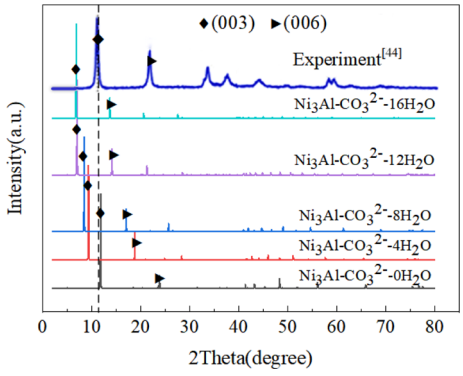

Figure 2. XRD simulation of Ni_3Al-CO_3^{2-}-LDH with different water contents.

it is revealed that as the number of water molecules increases, the (003) and (006) peaks, which represent the interlayer spacing, gradually shift to the left. The interlayer spacing of the model without water molecules is very close to the position of the (003) peak measured experimentally after drying, indicating that the calculated model without water molecules is consistent with the experimental results. It proves that the model design is correct and reasonable. The interlayer spacing gradually increased when the number of water molecules gradually increased, which is consistent with the results of the experimental study by Chen et al.[46] This literature reported a significant increase in interlayer water absorption and a gradual increase in interlayer spacing with increasing relative humidity

https://doi.org/10.1021/acsomega.2c06872
ACS Omega 2023, 8, 3286−3297

(RH) and immersion time in aqueous solutions. It is also consistent with the computational simulation results of Yan et al.[47] Therefore, the computational model designed in this paper is accurate and reasonable.

3.1. Interlayer Guest Arrangements. *3.1.1. Anion Arrangement.* The optimized results of the interlayer guest carbonate arrangement in the interlayer for the anhydrous interlayer model are presented in Figure 3. From Figure 3a, it

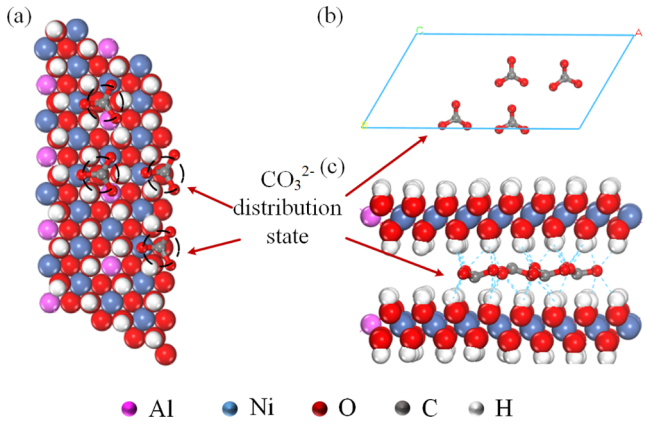

Figure 3. Anion arrangement after equilibrium of anhydrous molecules. (a) Top view of the model; (b) CO_3^{2-} arrangement; and (c) side view of the model.

can be established that CO_3^{2-} (circled in interlayer) is near the basal layer's hydroxyl group, and the carbonate's oxygen atoms are all above the cations of the basal layer. Figure 3b,c shows that the CO_3^{2-} and the basal layer are close to the parallel arrangement, and the statistical results of bond length and bond angle distribution of CO_3^{2-} are shown in Figure 4a,b. The bond length distribution state of CO_3^{2-} has proven to be longer than the theoretical bond length of 1.3 Å. The bond angle distribution is concentrated on the theoretical value of 120°.[29] O atoms in this arrangement of CO_3^{2-} interact with the basal layer H atoms by hydrogen bonding, the structure has lower energy, and the basal layer structure remains stable, in agreement with the literature results.[48] It also shows that hydrogen bonding only changes the C−O bond length of CO_3^{2-} and not the O−C−O bond angle. When the layer contains water molecules, the CO_3^{2-} position shifts, and the attitude is no longer parallel to the plate (Figure 4d).

3.1.2. Water Molecular Arrangement and Hydrogen Bonding. As shown in Figure 6, as the number of water molecules increases, N_w = 0, 4, 8, 12, 16, 20, 30, 35, and 40, the water molecules are arranged in one or more layers to form a laminar structure among the layers. Local magnification is shown in Figure 4c, the O atoms of the water molecules near the basal layer and H atoms near the CO_3^{2-} interlayer. In addition, from Figure 4c, when the number of water layers is more than 4, the interlayer water close to the basal layer is regularly arranged. The interlayer water away from the basal layer is less regularly arranged, caused by the hydrogen bonding between the water molecules, CO_3^{2-}, and the basal layer. It can be seen from Figure 4d that the Ni_3Al-CO_3^{2-}-LDH-nH_2O system has a complex hydrogen-bonding network with multiple hydrogen bonds. The distribution of bond lengths from H atoms to O atoms between the basal layer, anion, and water was analyzed using O atoms in the Ni_3Al-LDH structural model as a benchmark. The reference shows that bond lengths less than 2.45 Å are hydrogen bonds.[30] Here, the hydrogen bonds were divided into four types: A−L type (anion and basal layer), A−W type (anion and water), W−L type (water and basal layer), and W−W type (water and water), as can be observed in Figure 4d, as the number of water molecules increases, CO_3^{2-} gradually shifts from interacting with the basal layer to hydrate with water molecules and entering the hydrogen bonding network formed by water molecules. Under the action of the water molecule, the hydrogen bond network and the action between the water molecule and the basal layer, the interlayer anions, and the water molecules are arranged as mentioned above. This is demonstrated by the radial distribution function of H relative to O (e.g., Figure 5). The abscissa is less than 2.45 Å, and the ordinate value represents the average number of hydrogen bonds.

(1) Figure 5a shows that characteristic peaks of the A−L type hydrogen bonds gradually decrease with the increase of water molecular numbers N_w. It indicates that the anions gradually detach from the basal layers as the water molecular number increases and the LDH undergoes swelling.

(2) Figure 5b shows that characteristic peaks of A−W type hydrogen bonds with the increase in the number of water molecules appear to increase and then decrease. The maximum value occurs at N_w = 16. When the anion begins to hydrate with water molecules, it reaches the formation of a hydrogen-bonding network with water molecules, as shown in Figure 4d. When N_w exceeds 32, the action of the anion and water reaches a certain equilibrium state, as shown in Table 1 and Figure S3.

(3) Figure 5c shows that with the increase in the number of water molecules, the characteristic peaks of W−L type hydrogen bonds do not change significantly.

Combining with Figure 4c, it can be found that water molecules form ordered structural water layers, and the proportion of water molecules in the adjacent basal layer tends to be stable, so the characteristic peak of the W−L hydrogen bond fluctuates less.

(4) It can be seen in Figure 5d that the characteristic peaks of W−W hydrogen bonds do not increase with the increase of water molecule number. However, with the increase in water molecule number, the characteristic peak gradually moves to the left, indicating that the hydrogen bond length gradually shortens. In general, hydrogen bonds are directional and saturated, and the shorter the bond length of a hydrogen bond, the stronger the hydrogen bond.[25]

(5) Combining Figure 5a−d, it can be found that the properties of these four hydrogen bonds vary with the water molecules. When there are fewer water molecules, the hydrogen bonds are mainly of A−L type, indicating that the anion starts to have strong interactions with the layer; when the number of water molecules gradually increases, the water molecules break the hydrogen bonds between the anion and the hydrocarbon group of the layer and progressively shift to A−W type. In addition, hydrogen bonds are also generated between water molecules and hydrocarbon groups on the surface of the layer and water molecules. The final results show that the A−L type hydrogen bonding gradually decreases, and the A−W type hydrogen bonding

https://doi.org/10.1021/acsomega.2c06872
ACS Omega 2023, 8, 3286−3297

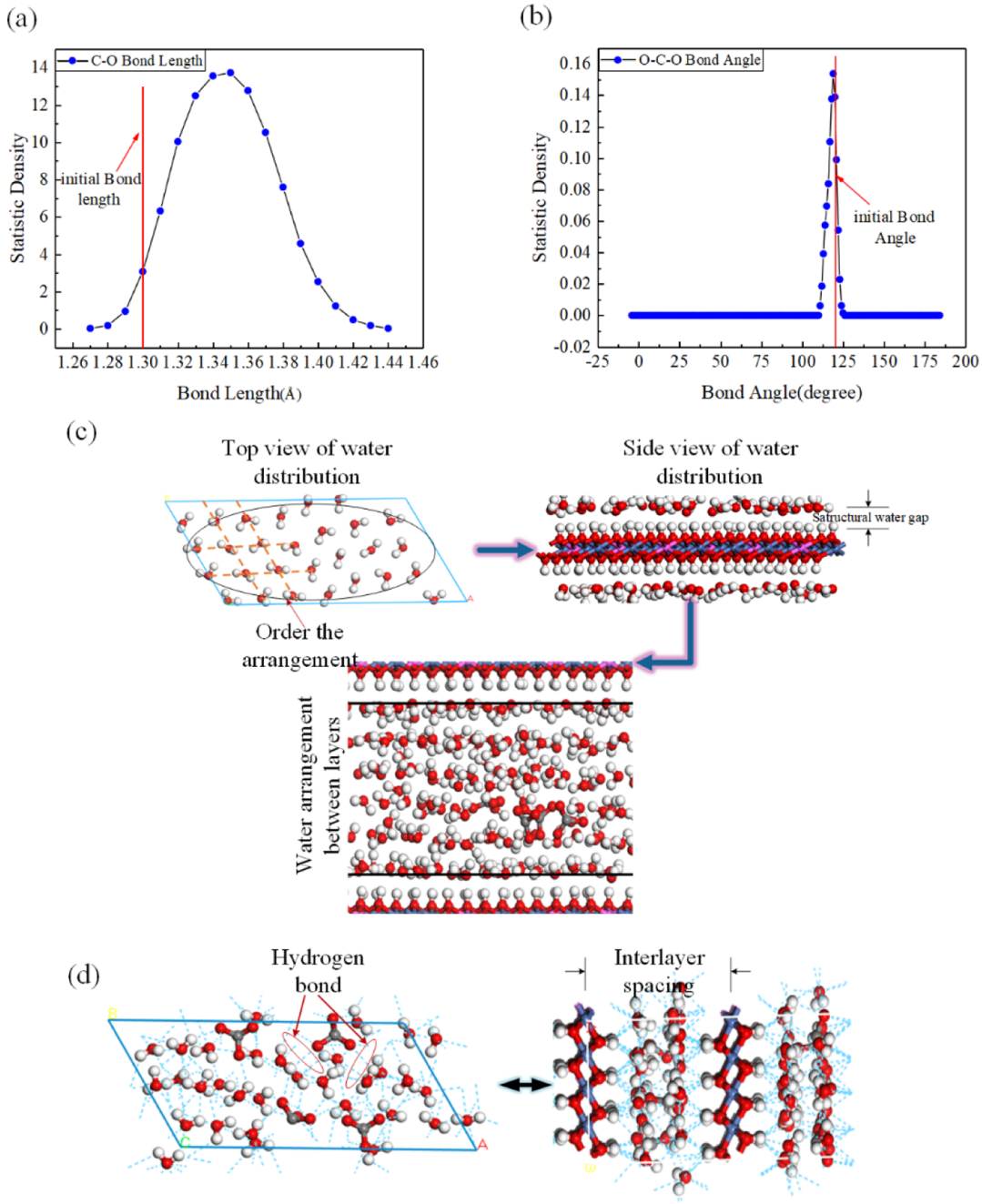

Figure 4. (a,b) Statistics of bond length−bond angle distribution of CO_3^{2} root ions at = 40; (c) interlayer arrangement of water molecules near the plating layer; and (d) hydrogen bonding network.

gradually increases. In addition, the W−L and W−W type hydrogen bonding gradually tends to a stable state.

After further calculation of the average number of the four hydrogen bond types, it is summarized in Table 1 and Figure S3. Combined with Figure 5, the relationship of hydrogen bonding on LDHs can be analyzed qualitatively and quantitatively, improving the results' reliability.

3.2. Analysis of the Basal Layer Structure and Swelling Structure. Under the different number of water molecules between layers, the optimization results of the LDH structure are shown in Figure 6. When water molecules are introduced to the interlayer, the interlayer spacing becomes larger due to the hydration of the swelling effect. The more water molecules, the larger the interlayer spacing. However, these two factors are not linear relationships. When fewer water molecules interlayer, the anions are mainly bound to the basal layer in a near-horizontal state, and the water molecules fill the gaps among the anions. The anion gradually tilts when the number of introducing water molecules is large. Also, the water molecules tend to bind the basal layer and form an orderly arrangement of structured water layers. In addition, the oxygen atoms of water molecules are oriented toward the basal layer and interact with the basal layer hydroxyl groups. The minimum angle between the anion and the basal layer is 1.103°, the maximum angle is close to the vertical, with the basal layer at 89.577°, and the average angle is about 45.34°. When N_w < 8, water molecules mainly fill the anion gap, and anions are in the middle of the layer; when N_w > 8, the anion

https://doi.org/10.1021/acsomega.2c06872
ACS Omega 2023, 8, 3286−3297

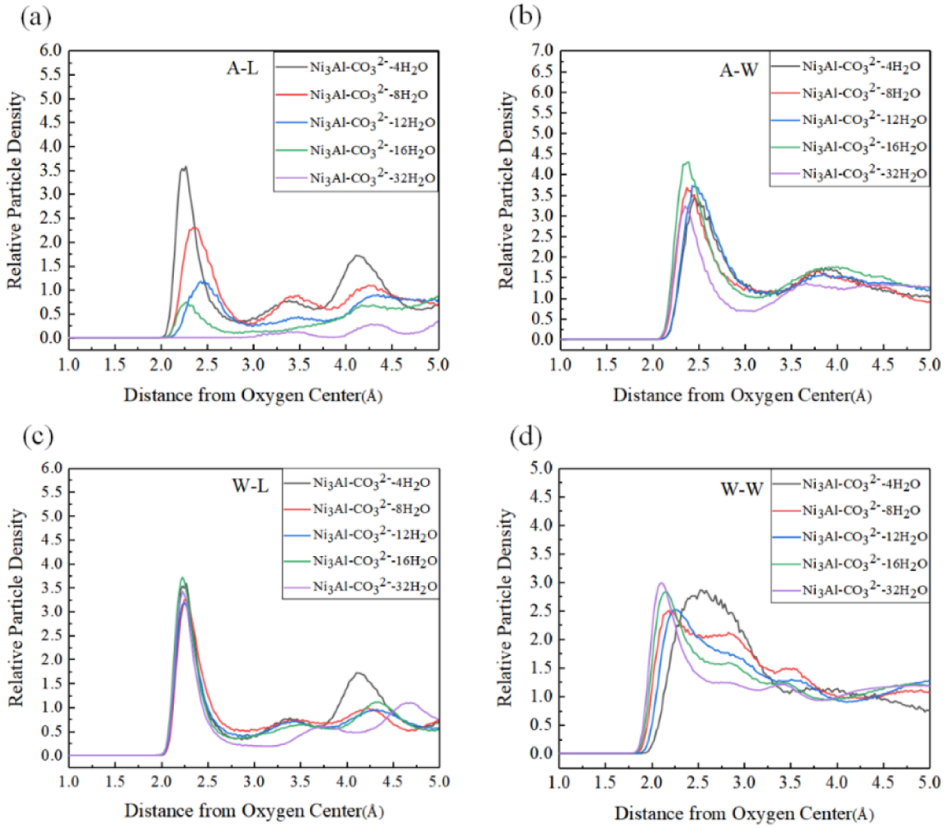

Figure 5. RDF diagrams of the four hydrogen bonding types. (a) A−L-type hydrogen bond; (b) A−W-type hydrogen bond; (c) W−L-type hydrogen bond; and (d) W−W-type hydrogen bond.

Table 1. Average Values of Various Hydrogen Bonds for Different Numbers of Water Molecules

	the average number of hydrogen bonds for the four hydrogen bond types[a]			
interlayer water molecules/N_w	A−L	A−W	W−L	W−W
0	6.673	0.000	0.000	0.000
4	5.618	4.555	1.873	1.478
8	3.812	5.937	1.742	1.535
12	1.893	5.031	1.531	1.471
16	1.214	6.770	1.531	1.701
20	1.817	4.877	1.531	1.839
32	0.003	5.360	1.531	1.661

[a]Note: The number of hydrogen bonds in each anion, a layer hydrocarbon group, and a water molecule. The number of hydrogen bonds containing anions is three times the average value.

gap is filled. The remaining water molecules are distributed on both sides of the basal layer to form a structural water layer. The average gap between water molecule layers, Δd_w (as shown in Table 2), provide a quantitative description of the water molecule arrangement. Figure 6 confirms that the increase in water molecules leads to interlayer swelling. Still, Table 2 shows that the structural water layer gap Δd_w gradually decreases, indicating a specific limit to the interlayer swelling. Variation of interlayer water molecule content versus LDH monolayer spacing is plotted in Figure 7a. The water molecular number has a relatively significant effect on the interlayer spacing d_c. When $N_w < 8$, there is only one abrupt change in the interlayer spacing, which remains essentially flat; when $8 < N_w < 24$, the interlayer spacing gradually increases rapidly with the increase of the number of introduced water molecules; after $N_w > 24$, the interlayer spacing tends to increase slowly and gradually stabilize. This can also prove that the swelling of LDHs is not infinite but has a specific limit. The hydration, swelling, structure, and kinetic of layered double hydroxides were experimentally investigated by Hou et al.[49] The results show that in the LDH-CO_3^{2-} system, water, hydroxyl groups, and carbonates have strong interactions and form a complex hydrogen bonding network between the LDH. When the LDH-CO_3^{2-} system is saturated with water, the strong interaction between the hydroxyl groups on the surface of the LDH layer and the interlayer water and carbonate prevents further insertion of water at high relative humidity. It agrees with the results calculated in this paper. In addition, Perotti et al.[50] found that the interlayer space of F-LDH-CMC was related to humidity. The swelling process in the interlayer space of LDH-CMC is due to the positive effect of the presence of hydrophilic carboxymethyl cellulose chains. As the humidity increases, the number of water molecules entering the interlayer space increases, causing interlayer swelling. Maximum layer spacing is reached when the relative humidity reaches 100%. These are in high agreement with the results affecting the expansion properties of LDHs studied by our paper calculations.

Does the occurrence of LDH interlayer swelling have some influence on the basal layer? The unit cell parameter a, as well as the O−M−O bond angle and O−M bond length in the base layer, was measured to study the effect of increasing the number of water molecules on the structure of the basal layer (M is the metal cation and O is the oxygen atom on the basal layer); the results are shown in Figure 7b,c. The unit cell

https://doi.org/10.1021/acsomega.2c06872
ACS Omega 2023, 8, 3286−3297

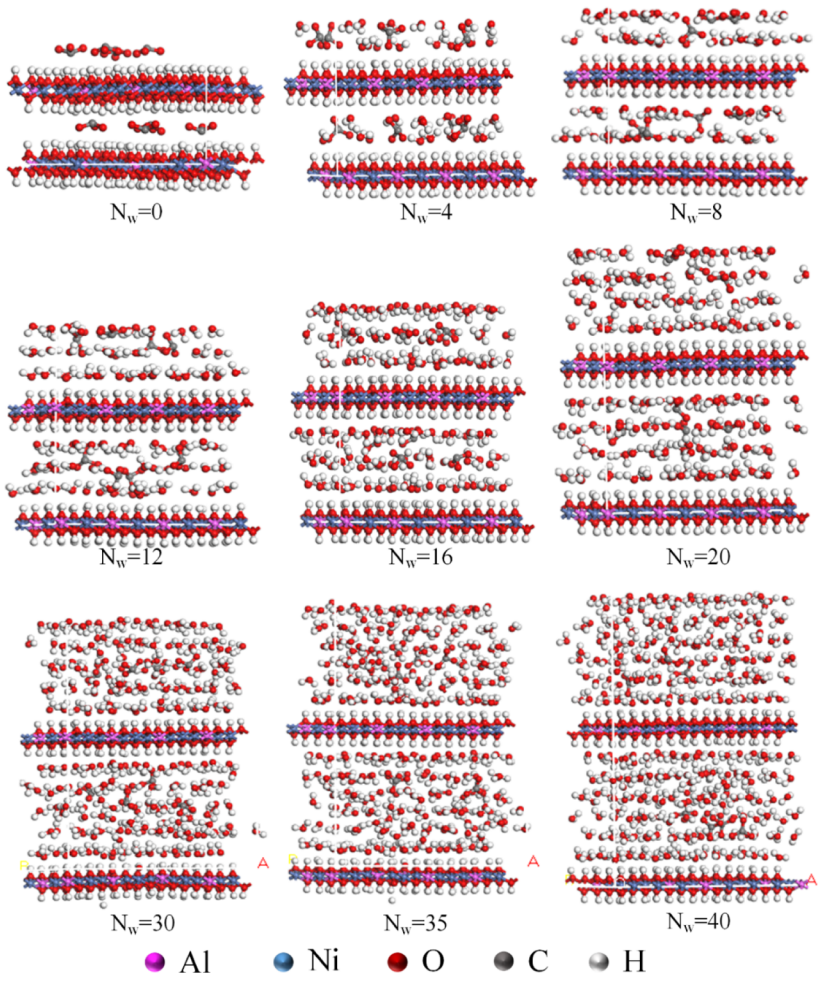

Figure 6. Ni_3Al-CO_3^{2-}-LDH hydrotalcite structure with the number of water molecules.

Table 2. Ni_3Al-CO_3^{2-}-LDH Interlayer Relative Water Layer Spacing

interlayer water molecules/N_w	0−7	8	12	16	20	25	30	35	40
relative aquifer gap/Δd_w (Å)[a]	-	0.108	0.065	0.051	0.038	0.029	0.025	0.019	0.017

[a]Note: The gap ratio between water molecules layers (Δd_w) is calculated by dividing the average gap of a single water layer by the number of water molecules between basal layers.

parameter *a* calculated from the *NPT* system with a minimum value of 2.51 Å and a maximum value of 3.07 Å is generally comparable to the crystallographic data of 3.04 Å reported in the literature.[42] As the number of water molecules increases, the cell parameter *a* shows an increasing trend. Combined with Figure 7c, it is found that both the O−M−O bond angle and O−M bond length in the basal layer gradually increases with the increase of water molecular number. It indicates that Ni_3Al-LDH with more water molecules exhibits a Ginger-Taylor effect. The distortion of the basal layer increases with the rise of the number of water molecules, which also proves that the stability of the LDH structure gradually decreases with the swelling.

3.3. Interlayer Hydration and Stability. *3.3.1. Interlayer Hydration.* Interlayer water molecules have an important influence on the structure and swelling properties of LDHs, and so, hydration energy is used to analyze the effect of introducing water molecules on the structure and properties of LDHs. The hydration energy is defined[32,51] as follows

$$\Delta U_H = \frac{U(N_w) - U(0)}{n} \quad (1)$$

where n is the total number of water molecules, $U(N_w)$ is the total potential energy of the system, and $U(0)$ is the total potential energy of the system when there are no water molecules. This equation can easily and effectively calculate the hydration energy of interlayer water.

The relationship between the hydration energy ΔU_H of Ni_3Al-CO_3^{2-}-LDHs and its degree of hydration (N_w) is shown in Figure 8. The hydration energy is the most negative when $N_w < 4$. The absolute value of hydration energy decreases faster as the number of introduced water molecules increases; when $N_w > 16$, the decreasing trend becomes slower. No local maxima of hydration energy was found throughout the hydration process. The phenomenon was as opposed to the previous simulation concerning simple inorganic anion intercalated LDHs (e.g., LDHs-Cl^-).[52] It can also be seen from the figure that for $N_w \leq 30$, Ni_3Al-CO_3^{2-}-LDH can continuously absorb water due to $\Delta U_H < -10$ kcal·mol^{-1} (the potential energy of bulk water is −10 kcal·mol^{-1}), resulting in

https://doi.org/10.1021/acsomega.2c06872
ACS Omega 2023, 8, 3286−3297

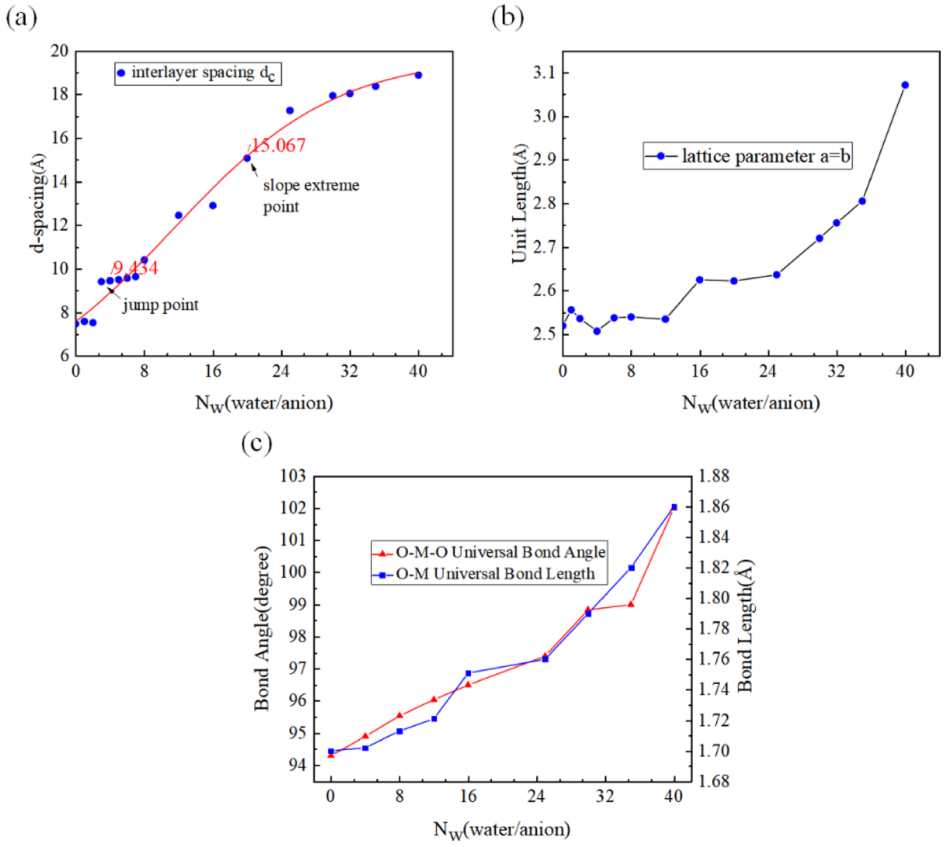

Figure 7. (a) Layer spacing of Ni_3Al-CO_3^{2-}-LDH; (b) unit cell parameters; and (c) variation of O−M bond length and O−M−O bond angle of the slab.

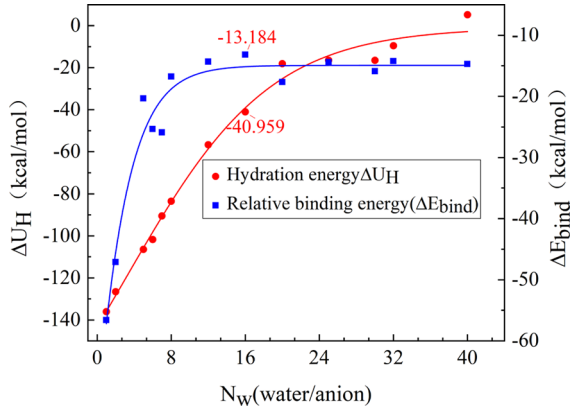

Figure 8. Hydration energy ΔU_H and relative binding energy of Ni_3Al-CO_3^{2-}-LDH.

the continuous expansion of the interlayer spacing; when N_w > 32, at this point $\Delta U_H > -10$ kcal·mol^{-1}, the potential energy in the bulk phase water state has been reached at this point according to the literature,[41,51] indicating that no further hydration can occur between the Ni_3Al-CO_3^{2-}-LDH layers. Therefore, the swelling of LDHs in the aqueous environment has a specific limit.

3.3.2. Structural Stability. The fundamental reason atoms combine into crystals is that the whole system has lower energy after the atoms combine. The energy is released during the binding of atoms from the free state into a crystal. It is the energy necessary to break up the crystal into individual free particles, called the crystal's binding energy.[53] To theoretically investigate the effect of the addition of water molecules on the stability of Ni_3Al-LDH, the relative binding energies of the Ni_3Al-CO_3^{2-}-LDH system at different N_w were calculated separately and defined as ΔE_{bind}

$$\Delta E_{bind} = \frac{E_{final} - E_{initial}}{N_w} \quad (2)$$

where N_w is the ratio of the number of water molecules to the number of anions, $E_{initial}$ is the sum of the energy of the atoms in the initial model, and E_{final} is the energy of the geometrically optimized system. The calculated results are shown in Figure 8. With the gradual increase of water molecule introduction, the absolute value of the relative binding energy of the system gradually decreases. We fit using Boltzmann's equation. When N_w < 8, the absolute value of the binding energy drops sharply with increases in water molecular number, and the stability starts to decrease; after N_w > 12, the relative binding energy starts to converge to −14 kcal·mol^{-1} as increases in the number of water molecules and no longer changes significantly. The structure remains lowly stable when the interlayer water molecule N_w > 12. Figure 7a,d concludes that the structural stability first decreases and then tends to equilibrium. Because of the increase in water molecules, the interlayer spacing of LDHs increases due to the rapid swelling, and the structural stability also decreases rapidly. In N_w > 24, the swelling rate begins to decline. When N_w = 32, hydration energy can reach the potential energy of the bulk water −10 kcal·mol^{-1}. Interlayer hydration is no longer spontaneously generated, and the interlayer water is saturated. In addition, another piece of evidence for the decrease of structural stability due to

https://doi.org/10.1021/acsomega.2c06872
ACS Omega 2023, 8, 3286−3297

swelling is that the relationship between the relative binding energy and the interlayer spacing (Table 3) exhibits a similar variation pattern to that shown in Figure 8.

Table 3. Correlation of Layer Spacing (d_c) With Relative Binding Energy (ΔE_{bind})

layer spacing/d_c (Å)	relative binding energy/ΔE_{bind}(kcal·mol^{-1})
7.561	−56.602
7.502	−47.132
9.549	−25.352
9.626	−25.912
10.388	−16.768
12.439	−14.328
12.885	−13.184
17.255	−14.416
17.934	−15.881
18.035	−14.232
18.881	−14.712

3.4. Diffusion of Anions. Anion diffusion is usually used in studying the mechanism of ion exchange. Therefore, in this paper, the magnitude of the diffusion rate of interlayer anions at different states of water molecular number is investigated based on the equation of the diffusion rate D_A versus the root mean square displacement (MSD)[54]

$$D_A = \frac{1}{6}\lim_{t\to\infty}([r(t) - r(0)]^2) \quad (3)$$

the mean squared displacement curve function $r(t)$ is indicated, the specific data of the calculation are shown in Table S4, and the diffusion rate D_A is shown in Figure 9. When N_w = 4, 16, and 35, the interlayer anion diffusion rate of Ni_3Al-LDH exhibits a local maximum value. The maximum peak at N_w = 4 in Figure 9b may be because water molecules reduce the interaction between anions and the basal layer and increase the interaction with water molecules, which enhances the mobility of anions. Water molecules increase further, and the anion diffusion rate decreases due to steric hindrance. It can be inferred from Figure 7a that when N_w < 8, the interlayer spacing is slightly increased, and the steric hindrance of a few water molecules (N_w = 4) interlayers is small, resulting in an extreme value of the anion diffusion rate. As the interlayer spacing increases, the diffusion coefficient reaches a maximum of 10.97 × 10^{-8} cm^2·s^{-1} when N_w = 16 due to the water molecules forming a layer structure with large gaps (Figure 6). When N_w > 16, according to Table 3 and Figure 5, the distance between water molecules decreases, the steric hindrance of water molecules becomes more significant, and the interlayer anion diffusion rate of Ni/Al-LDH begins to show a slow downward trend.

The abovementioned phenomenon indicates that an appropriate number of water molecules in the LDH interlayer can promote anion movement. However, when the number of water molecule interlayer exceeds a specific value, the diffusion rate of anions decreases due to steric hindrance. In this paper, it is found that Ni_3Al-LDH reaches the maximum interlayer anion diffusion rate when N_w = 16, indicating that the ion exchange efficiency is the highest at this time.

4. CONCLUSIONS

The swelling structure, hydration characteristics, binding energy, and anion diffusion properties of Ni_3Al-LDH were studied by molecular dynamics simulation.

(1) The interlayer water molecules of Ni_3Al-LDH present a regular layered arrangement, and the interlayer anions are in the water molecule layer and combine with the water molecules by hydrogen bonds.

(2) As the number of water molecules increases, the hydrogen bond between the anion and the basal layer gradually weakens and disappears when the number of water molecules is 32. The hydrogen bond between the anion and the water molecule gradually increases, reaching an extreme value when the number of water molecules is 16.

(3) The interlayer spacing of Ni_3Al-LDH is not linear with the number of water molecules. The interlayer spacing increases slowly when the number of water molecules is more than 24. The maximum layer spacing is stable at around 19 Å.

(4) The results of interlayer spacing, binding energy, and hydration energy all show an upper limit for swelling; that is, the number of water molecules is 32. When $N_w \leq$ 30, Ni_3Al LDH can continuously absorb water due to ΔU_H being smaller than the potential energy of bulk water −10 kcal·mol^{-1}, resulting in the continuous expansion of the material interlayer spacing. When N_w > 32, the Ni_3Al LDH interlayer cannot be further

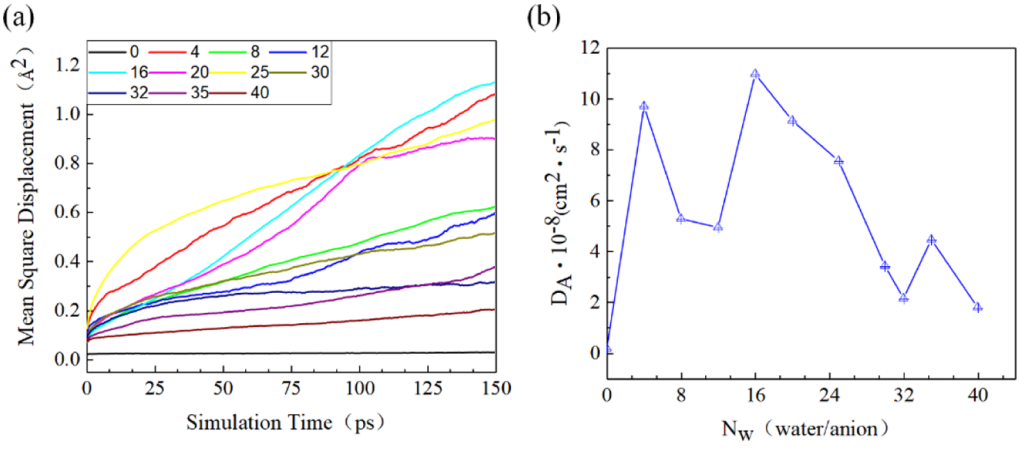

Figure 9. (a) Mean squared displacement of Ni_3Al-CO_3^{2-}-LDH with different water molecular numbers and (b) CO_3^{2-} diffusion rate.

https://doi.org/10.1021/acsomega.2c06872
ACS Omega 2023, 8, 3286−3297

spontaneously hydrated. The binding energy is stable at around −14 kcal·mol^{-1}.

(5) When the number of interlayer water molecules is 16, the water molecules' layer structure and LDH interlayer spacing are suitable for anions to obtain the maximum diffusion rate, 10.97 × 10^{-8} cm^2·s^{-1}.

■ ASSOCIATED CONTENT

Supporting Information

The Supporting Information is available free of charge at https://pubs.acs.org/doi/10.1021/acsomega.2c06872.

Error analysis of Ni_3Al-CO_3^{2-}-LDH model calculation cutoff distance accuracy confirmation, lattice parameters under different simulation times, interlayer diffusion coefficients of CO_3^{2-} under the action of different interlayer water molecules, geometric structure diagrams of simulations under different force fields, energy variation diagrams under different simulation times, and folding diagrams of average number variation of four hydrogen bonds under different water molecule numbers (PDF)

■ AUTHOR INFORMATION

Corresponding Authors

Xiaoliang Wang − *College of Materials Science and Engineering, Key Laboratory of Mineral High Value Conversion and Energy Storage Materials of Liaoning Province, Geology and Mineral Engineering Special Materials Professional Technology Innovation Center of Liaoning Province, Liaoning Technical University, Fuxin 123000, China;* orcid.org/0000-0003-3508-856X; Phone: 13704181324; Email: ningke@163.com

Shaobin Yang − *College of Materials Science and Engineering, Key Laboratory of Mineral High Value Conversion and Energy Storage Materials of Liaoning Province, Geology and Mineral Engineering Special Materials Professional Technology Innovation Center of Liaoning Province, Liaoning Technical University, Fuxin 123000, China;* Phone: 13941862976; Email: lgdysb@163.com

Authors

Leiming Chang − *College of Materials Science and Engineering, Key Laboratory of Mineral High Value Conversion and Energy Storage Materials of Liaoning Province, Geology and Mineral Engineering Special Materials Professional Technology Innovation Center of Liaoning Province, Liaoning Technical University, Fuxin 123000, China*

Haonan Zhao − *College of Materials Science and Engineering, Key Laboratory of Mineral High Value Conversion and Energy Storage Materials of Liaoning Province, Geology and Mineral Engineering Special Materials Professional Technology Innovation Center of Liaoning Province, Liaoning Technical University, Fuxin 123000, China*

Zhenqiu Yu − *College of Materials Science and Engineering, Key Laboratory of Mineral High Value Conversion and Energy Storage Materials of Liaoning Province, Geology and Mineral Engineering Special Materials Professional Technology Innovation Center of Liaoning Province, Liaoning Technical University, Fuxin 123000, China*

Yingkai Xia − *College of Materials Science and Engineering, Key Laboratory of Mineral High Value Conversion and Energy Storage Materials of Liaoning Province, Geology and Mineral Engineering Special Materials Professional Technology Innovation Center of Liaoning Province, Liaoning Technical University, Fuxin 123000, China*

Chuanhui Huang − *School of Mechanical and Electrical Engineering, Xuzhou University of Technology, Xuzhou 221111, China*

Guoxiang Pan − *School of Engineering, Huzhou University, Huzhou 313000, China*

Shengjie Xia − *College of Chemical Engineering, Zhejiang University of Technology, Hangzhou 310014, China*

Yi Liu − *School of Mechanical and Electrical Engineering, Xuzhou University of Technology, Xuzhou 221111, China*

Jingxin Fan − *CCTEG China Coal Research Institute, Beijing 100013, China*

Complete contact information is available at: https://pubs.acs.org/10.1021/acsomega.2c06872

Notes

The authors declare no competing financial interest.

■ ACKNOWLEDGMENTS

The project was supported by National Natural Science Foundation of China (51974152), Natural Science Foundation of Liaoning Province, China (2019-ZD-0033). The project was supported by discipline innovation team of Liaoning Technical University (no. LNTU20TD-9 and LNTU20TD-16).

■ REFERENCES

(1) Rosenberg, S. P.; Armstrong, L.Layered Double Hydroxides in the Bayer Process: Past, Present and Future. *Essential Readings in Light Metals*; Springer, 2016; pp 235−239.

(2) Prasad, C.; Tang, H.; Liu, Q. Q.; Zulfiqar, S.; Shah, S.; Bahadur, I. An Overview of Semiconductors/Layered Double Hydroxides Composites: Properties, Synthesis, Photocatalytic and Photoelectrochemical Applications. *J. Mol. Liq.* **2019**, *289*, 111114.

(3) Mishra, G.; Dash, B.; Pandey, S. Layered Double Hydroxides: A Brief Review from Fundamentals to Application as Evolving Biomaterials. *Appl. Clay Sci.* **2018**, *153*, 172−186.

(4) Anantharaj, S.; Karthick, K.; Kundu, S. Evolution of Layered Double Hydroxides (LDH) as High Performance Water Oxidation Electrocatalysts: A Review with Insights on Structure, Activity and Mechanism. *Mater. Today Energy* **2017**, *6*, 1−26.

(5) Asif, M.; Aziz, A.; Azeem, M.; Wang, Z. Y.; Ashraf, G.; Xiao, F.; Chen, X. D.; Liu, H. F. A Review on Electrochemical Biosensing Platform Based on Layered Double Hydroxides for Small Molecule Biomarkers Determination. *Adv. Colloid Interface Sci.* **2018**, *262*, 21−38.

(6) Daud, M.; Hai, A.; Banat, F.; Wazir, M. B.; Habib, M.; Bharath, G.; Al-Harthi, M. A. A Review on the Recent Advances, Challenges and Future Aspect of Layered Double Hydroxides (LDH) - Containing Hybrids as Promising Adsorbents for Dyes Removal. *J. Mol. Liq.* **2019**, *288*, 110989.

(7) Lan, M.; Fan, G. L.; Chen, Q. L.; Li, F. Synthesis of Multi-Walled Carbon Nanotubes over Tungsten-Doped Cobalt-Based Catalyst Derived from a Layered Double Hydroxide Precursor. *J. Ind. Eng. Chem.* **2014**, *20*, 1523−1531.

(8) Menezes, J.; da Silva, T.; dos Santos, J.; Catari, E.; Meneghetti, M.; da Matta, C.; Alexandre-Moreira, M.; Santos-Magalhães, N.; Grillo, L.; Dornelas, C. Layered Double Hydroxides (LDHs) as Carrier of Antimony Aimed for Improving Leishmaniasis Chemotherapy. *Appl. Clay Sci.* **2014**, *91*−*92*, 127−134.

(9) Zhao, R. D.; Cui, D.; Dai, J. Q.; Xiang, J.; Wu, F. F. Morphology Controllable $NiCo_2O_4$ Nanostructure for Excellent Energy Storage Device and Overall Water Splitting. *Sustainable Mater. Technol.* **2020**, *24*, No. e00151.

(10) Cui, D.; Zhao, R. D.; Dai, J. Q.; Xiang, J.; Wu, F. F. A hybrid $NiCo_2O_4$@$NiMoO_4$ structure for overall water splitting and excellent hybrid energy storage. *Dalton Trans.* **2020**, *49*, 9668−9679.
(11) Yang, W. D.; Zhao, R. D.; Guo, F. Y.; Xiang, J.; Loy, S.; Liu, L.; Dai, J. Y.; Wu, F. F. Interface engineering of hybrid $ZnCo_2O_4$@$Ni_{2.5}Mo_6S_{6.7}$ structures for flexible energy storage and alkaline water splitting. *Chem. Eng. J.* **2023**, *454*, 140458.
(12) Ma, Y.; Wu, Z. J.; Wang, H. W.; Wang, G. Q.; Zhang, Y. K.; Hu, P. C.; Li, Y. M.; Gao, D. K.; Pu, H. Q.; Wang, B. Z.; et al. Synthesis of nanocrystalline strontium titanate by a sol-gel assisted solid phase method and its formation mechanism and photocatalytic activity. *CrystEngComm* **2019**, *21*, 3982−3992.
(13) Wang, H. W.; Wang, G. Q.; Zhang, Y. K.; Ma, Y.; Wu, Z. J.; Gao, D. K.; Yang, R. T.; Wang, B. Z.; Qi, X. W.; Yang, J. Preparation of RGO/TiO_2/Ag Aerogel and Its Photodegradation Performance in Gas Phase Formaldehyde. *Sci. Rep.* **2019**, *9*, 16314.
(14) Yang, W. D.; Zhao, R. D.; Xiang, J.; Loy, S.; Di, Y. F.; Li, J.; Li, M. T.; Ma, D. M.; Wu, F. F. 3D hierarchical $ZnCo_2S_4$@$Ni(OH)_2$ nanowire arrays with excellent flexible energy storage and electrocatalytic performance. *J. Colloid Interface Sci.* **2022**, *626*, 866−878.
(15) Gao, X.; Wang, P. K.; Pan, Z. H.; Claverie, J. P.; Wang, J. Recent Progress in Two-Dimensional Layered Double Hydroxides and Their Derivatives for Supercapacitors. *ChemSusChem* **2020**, *13*, 1226−1254.
(16) Zha, D. S.; Sun, H. H.; Fu, Y. S.; Ouyang, X. P.; Wang, X. Acetate Anion-Intercalated Nickel-Cobalt Layered Double Hydroxide Nanosheets Supported on Ni Foam for High-Performance Supercapacitors with Excellent Long-Term Cycling Stability. *Electrochim. Acta* **2017**, *236*, 18−27.
(17) Liu, X.; Ma, R. Z.; Bando, Y.; Sasaki, T. A General Strategy to Layered Transition-Metal Hydroxide Nanocones: Tuning the Composition for High Electrochemical Performance. *Adv. Mater.* **2012**, *24*, 2148−2153.
(18) Therias, S.; Mousty, C.; Forano, C.; Besse, J. P. Electrochemical Transfer at Anionic Clay Modified Electrodes. Case of 2,2′-Azinobis(3-ethylbenzothiazoline-6-sulfonate). *Langmuir* **1996**, *12*, 4914−4920.
(19) Liu, X. M.; Zhang, L.; Gao, X. R.; Guan, C.; Hu, Y. T.; Wang, J. Enlarged Interlayer Spacing in Cobalt-Manganese Layered Double Hydroxide Guiding Transformation to Layered Structure for High Supercapacitance. *ACS Appl. Mater. Interfaces* **2019**, *11*, 23236−23243.
(20) Xiao, Y. H.; Su, D. C.; Wang, X. Z.; Wu, S. D.; Zhou, L. M.; Fang, S. M.; Li, F. Layered Double Hydroxides with Larger Interlayer Distance for Enhanced Pseudocapacitance. *Sci. China Mater.* **2017**, *61*, 263−272.
(21) Lin, Y. Y.; Xie, X. L.; Wang, X.; Zhang, B.; Li, C. J.; Wang, H.; Wang, L. J. Understanding the Enhancement of Electrochemical Properties of NiCo Layered Double Hydroxides Via Functional Pillared Effect: An Insight into Dual Charge Storage Mechanisms. *Electrochim. Acta* **2017**, *246*, 406−414.
(22) Ding, D.; Song, X.; Wei, C. L.; Hu, Z. H.; Liu, Z. Y. Efficient Sorptive Removal of F-53B from Water by Layered Double Hydroxides: Performance and Mechanisms. *Chemosphere* **2020**, *252*, 126443.
(23) Zhang, C. J.; Tsuboi, T.; Namba, H.; Einaga, Y.; Yamamoto, T. Enhancement of the Coercivity in Co-Ni Layered Double Hydroxides by Increasing Basal Spacing. *Dalton Trans.* **2016**, *45*, 13324−13331.
(24) Wang, X. L.; Li, Z.; Zhang, J. Q.; Yanyan, H.; Wang, C.; Wu, F. Q.; Tian, A. N.; Hong, X. D.; Dong, W.; Yang, S. B. Effect of Average Interlayer Spacing on Capacitance of NiMn Layered Double Hydroxide. *Chem. Eng. J.* **2020**, *398*, 125618.
(25) SHI, W.; HU, J.; NI, Z. M.; LI, Y.; LIU, J. Influence of Interlayer Water Content on Supermolecular Interaction of Copper-Iron Layered Double Hydroxides. *Acta Phys.-Chim. Sin.* **2012**, *28*, 1869−1876.
(26) Murthy, V.; Smith, H. D.; Zhang, H.; Smith, S. C. Molecular Modeling of Hydrotalcite Structure Intercalated with Transition Metal Oxide Anions: CrO_4^{2-} and VO_4^{3-}. *J. Phys. Chem. A* **2011**, *115*, 13673−13683.
(27) Costa, D. G.; Rocha, A. B.; Diniz, R.; Souza, W. F.; Chiaro, S. S. X.; Leitão, A. A. Structural Model Proposition and Thermodynamic and Vibrational Analysis of Hydrotalcite-Like Compounds by DFT Calculations. *J. Phys. Chem. C* **2010**, *114*, 14133−14140.
(28) Costa, D. G.; Rocha, A. B.; Souza, W. F.; Chiaro, S. S. X.; Leitão, A. A. Comparative Structural, thermodynamic and electronic analyses of Zn-Al-A^n- hydrotalcite-like compounds (A^n=Cl^-, F^-, Br^-, OH^-, CO_3^{2-} or NO_3^-): An ab initio study. *Appl. Clay Sci.* **2012**, *56*, 16−22.
(29) Costa, D. G.; Rocha, A. B.; Souza, W. F.; Chiaro, S. S. X.; Leitão, A. A. Ab Initio Simulation of Changes in Geometry, Electronic Structure, and Gibbs Free Energy Caused by Dehydration of Hydrotalcites Containing $Cl^-$and CO_3^{2-}Counteranions. *J. Phys. Chem. B* **2011**, *115*, 3531−3537.
(30) Chen, M.; Shen, W.; Lu, X. C.; Zhu, R. L.; He, H. P.; Zhu, J. X. Jumping Diffusion of Water Intercalated in Layered Double Hydroxides. *J. Phys. Chem. C* **2016**, *120*, 12924−12931.
(31) Marappa, S.; Vishnu Kamath, P. Water Molecules in Hydrotalcite-Like Layered Double Hydroxides: Interplay between the Hydration of the Anions and the Metal Hydroxide Layer. *Z. Anorg. Allg. Chem.* **2015**, *641*, 927−934.
(32) Li, X. J.; Würger, T.; Feiler, C.; Meißner, R. H.; Serdechnova, M.; Blawert, C.; Zheludkevich, M. L. Atomistic Insight into the Hydration States of Layered Double Hydroxides. *ACS Omega* **2022**, *7*, 12412−12423.
(33) Dias, A.; Cunha, L.; Vieira, A. C. Synthesis and properties of $A_6B_2(OH)_{16}Cl_2{\cdot}4H_2O$ (A = Mg, Ni, Zn, Co, Mn and B = Al, Fe) materials for environmental applications. *Mater. Res. Bull.* **2011**, *46*, 1346−1351.
(34) PAN, G. X.; NI, Z. M.; WANG, F.; WANG, J. G.; LI, X. N. Molecular Dynamics Simulation on Structure, Hydrogen-Bond and Hydration Properties of Diflunisal Intercalated Layered Double Hydroxides. *Acta Phys.-Chim. Sin.* **2009**, *25*, 223−228.
(35) Ding, S. Q.; Du, X.; Yang, Y. Y.; Wang, P. F.; Zhang, Z. L.; Hao, X. G.; Peng, C. J.; Guan, G. Q. Theoretical and experimental investigations of the electronic/ionic conductivity and deprotonation of $Ni_{3-x}Co_xAl$-LDHs in an electrochemical energy storage system. *Phys. Chem. Chem. Phys.* **2018**, *20*, 17313−17323.
(36) Cao, L. R.; Zhang, C. Y.; Zhang, D. L.; Chu, H. Y.; Zhang, Y. B.; Li, G.-H. Recent Developments in Using Molecular Dynamics Simulation Techniques to Study Biomolecules. *Acta Phys.-Chim. Sin.* **2017**, *33*, 1354−1365.
(37) Berendsen, H. J. C.; Postma, J. P. M.; van Gunsteren, W. F.; Hermans, J. Interaction Models for Water in Relation to Protein Hydration. *Intermol. Forces* **1981**, *14*, 331−342.
(38) Parrinello, M.; Rahman, A. Polymorphic Transitions in Single Crystals: A New Molecular Dynamics Method. *J. Appl. Phys.* **1981**, *52*, 7182−7190.
(39) Askar, A.; Space, B.; Rabitz, H. Subspace Method for Long Time Scale Molecular Dynamics. *J. Phys. Chem.* **1995**, *99*, 7330−7338.
(40) Kalinichev, A. G.; Padma Kumar, P.; James Kirkpatrick, R. Molecular Dynamics Computer Simulations of the Effects of Hydrogen Bonding on the Properties of Layered Double Hydroxides Intercalated with Organic Acids. *Philos. Mag.* **2010**, *90*, 2475−2488.
(41) Padma Kumar, P.; Kalinichev, A. G.; James Kirkpatrick, R. Molecular Dynamics Simulation of the Energetics and Structure of Layered Double Hydroxides Intercalated with Carboxylic Acids. *J. Phys. Chem. C* **2007**, *111*, 13517−13523.
(42) Zhao, X. J.; Zhu, Y. Q.; Xu, S. M.; Liu, H. M.; Yin, P.; Feng, Y. L.; Yan, H. Anion exchange behavior of MIIAl layered double hydroxides: a molecular dynamics and DFT study. *Phys. Chem. Chem. Phys.* **2020**, *22*, 19758−19768.
(43) An, X.; Feng, C. Q.; Ren, J.; Shi, K.; Du, Y. L.; Xie, X. M.; Wu, X. Novel Highly Dispersed Ni-Based Oxides Catalysts for Ethanol Steam Reforming. *J. Energy Inst.* **2021**, *99*, 240−247.

https://doi.org/10.1021/acsomega.2c06872
ACS Omega 2023, 8, 3286−3297

(44) Lv, H.; Rao, H. B.; Liu, Z.; Zhou, Z. Y.; Zhao, Y.; Wei, H. L.; Chen, Z. X. NiAl Layered Double Hydroxides with Enhanced Interlayer Spacing Via Ion-Exchange as Ultra-High Performance Supercapacitors Electrode Materials. *J. Energy Storage* **2022**, *52*, 104940.
(45) Li, X.; HOU, Y. L.; WANG, Y. H. Preparation of Ni/Al Layered Double Hydroxides Nanosheet Filmonvarious Substrate. *J. Wuhan Univ. Sci. Technol.* **2020**, *43*, 419−423.
(46) Chen, C. P.; Ruengkajorn, K.; Buffet, J. C.; O'Hare, D. Water Adsorbancy of High Surface Area Layered Double Hydroxides (AMO-LDHs). *RSC Adv.* **2018**, *8*, 34650−34655.
(47) Yan, D. P.; Lu, J.; Wei, M.; Li, H.; Ma, J.; Li, F.; Evans, D. G.; Duan, X. In Situ Polymerization of the 4-Vinylbenzenesulfonic Anion in Ni−Al−Layered Double Hydroxide and Its Molecular Dynamic Simulation. *J. Phys. Chem. A* **2008**, *112*, 7671−7681.
(48) Miyata, S. Anion-Exchange Properties of Hydrotalcite-Like Compounds. *Clays Clay Miner.* **1983**, *31*, 305−311.
(49) Hou, X. Q.; Bish, D. L.; Wang, S. L.; Johnston, C. T.; James Kirkpatrick, R. Hydration, Expansion, Structure, and Dynamics of Layered Double Hydroxides. *Am. Mineral.* **2003**, *88*, 167−179.
(50) Perotti, G. F.; Bortotti, J. R.; Lima, F. S.; Michels, L.; dos Santos, E. C.; Altoé, M. A. S.; Grassi, G.; Silva, G. J.; Droppa-Jr, R., Jr; Fossum, J. O.; et al. Exfoliation of Carboxymethylcellulose-Intercalated Layered Double Hydroxide in Water. *Appl. Clay Sci.* **2021**, *205*, 106005.
(51) Padma Kumar, P.; Kalinichev, A. G.; James Kirkpatrick, R. Hydration, Swelling, Interlayer Structure, and Hydrogen Bonding in Organolayered Double Hydroxides: Insights from Molecular Dynamics Simulation of Citrate-Intercalated Hydrotalcite. *J. Phys. Chem. B* **2006**, *110*, 3841−3844.
(52) Wang, J. W.; Kalinichev, A. G.; James Kirkpatrick, R. Asymmetric Hydrogen Bonding and Orientational Ordering of Water at Hydrophobic and Hydrophilic Surfaces: A Comparison of Water/Vapor, Water/Talc, and Water/Mica Interfaces. *J. Phys. Chem. C* **2009**, *113*, 11077−11085.
(53) NI, Z.-M.; LI, Y.; SHI, W.; XUE, J.-L.; LIU, J. Supramolecular Structure, Electronic Property and Stability of Ni-Mg-Al Layered Double Hydroxides. *Acta Phys.-Chim. Sin.* **2012**, *28*, 2051−2056.
(54) Yi, Y.; Bi, P.; Zhao, X. F.; Wang, L. L. Molecular Dynamics Simulation of Diffusion of Hydrogen and Its Isotopic Molecule in Polystyrene. *J. Polym. Res.* **2018**, *25*, 43.

https://doi.org/10.1021/acsomega.2c06872
ACS Omega 2023, 8, 3286−3297